2D/3D Paraxial maximum field Green's funtion generator

Paulo E. M. Cunha PETROBRAS S/A

Abstract

The time seismographic interpretation can contain errors associated to the incorrect conformation of the seismic events. This fact can even carry economical losses due to exploratory or/and exploitatory well mis-positioning, or still hide a favorable prospecting situation. This is particularly evident in regions of great geological complexity and/or strong lateral velocity variations. The recent advances in the intensive computational technology with production of high computational capacity machines, particularly the parallel architectures, have woken up crescent attention to the depth imaging. The 2D/3D Paraxial Ray-Tracing (Popov, 1977) , (Popov and Pšenčik, 1978b), (Popov and Pšenčik, 1978a) will exert, among other functions, the 2D/3D *Green's* function simulator, acting as the heart of a series of applications, such as velocity analysis by reflexion tomographic inversion, AVA, *Kirchhoff* modeling, amplitude correction, etc. The 3D pre-stack depth migration *(PSDM)* will use the travel time table obtained by this procedure to implement the image condition to the *Kirchhoff's* integral imaging operator and, eventually, to the reverse time migration *(RTM)*.

This work presents the results of building the image condition by the solution of a system of 21 non linear first order differential *PARAXIAL* equations for dynamical ray tracing. This corresponds to a generalization of a kinematic version already developed (Cunha, 1999a), with adaptive step time control between the ray points. These travel times will be subsequently employed in the *Kirchhoff's* integral operator for *PSDM*. The evaluation of the image condition by solving a non linear first order differential equation (*EIKONAL's* method) (Faria and Stoffa, 1994) is in general fast, but presents some serious inconveniences, such as: a) High degree of instability in complex media (Popov, 2002) where *"Caustic"* phenomena will fatally occur, increasing by several orders of magnitude the rate of the error, even in points far from it. b) Determine only the first arrivals. c) Doesn't allow the determination of the maximum field's image condition since this requires evaluation of travel time for multiple arrivals. The main motivation for using *RTM* is to employ the full acoustical - elastic wave equation to propagate the stress field, where it is implicit the presence of a punctual *Green's* function centered in the source - receptor stations, which makes the implementation of the maximum field image condition *MFIC* natural and simple.

The experience with real data indicates that the *RTM* results for complex media are often superior than that obtained by other methods. However, its main limitation is the great computational cost which is proportional to the number of source - receptor points. The parallel processing, particularly *LINUX's Clusters*, (Soares, Filho and Bulcão, André and De Bragança, R. S. N., 2002) will gradually favor the conventional *RTM*, although the computational costs still have some impact. The use of coarse transverse grid (Mufti et al., 1996) (Cunha, 1997) can reduce the computational costs, but at the expense of problems like *numerical anisotropy* (Alford et al., 1974) (Cunha, 1999b). However, with the development of the "Multi Source" version of the *RTM* (Cunha, 2002) this seems no longer be true. We believe that part of this qualitative superiority could be credited just to the *MFIC*, as supported by this work.

Theoretical Foundations

The image condition $\tau_{s_j}(x,y,z)$ is the time necessary by the wave field to move from a punctual source s_j with coordinates $\vec{r}_{s_j}$ to each grid point $\vec{r}(x,y,z)$. The finite difference method is specially adequate to the building of *maximum field* image condition and to the amplitude correction. The method will follow the scheme described in the following code lines:

for all $(\vec{r},t)$ propagate $U(\vec{r},t)$
  if $U(\vec{r},t) > U_{max}(\vec{r})$
  then $U_{max}(\vec{r}) = U(\vec{r},t)$; $\tau(\vec{r}) = t$
  and if
and for $(\vec{r},t)$
$A(\vec{r}) = U_{max}(\vec{r},t)$

This simple code stage is capable to detect the time $\tau_{s_j}(\vec{r})$ needed by the maximum amplitude's field to move from the source to the scattering point $\vec{r}$, as well as to determine the amplitude correction, $A(\vec{r}) = U_{max}(\vec{r})$, for each point of the depth grid. However, the seismogram injection must be made at reverse time order, beginning with the last sample, which is the maximum time of register T_{max}, until the first sample. Then, the image condition of the source point s_j necessary to freeze the field shall be $\tau_{g_i}(\vec{r}) = T_{max} - \tau_{s_j}(\vec{r})$ (see figure-1-B) which corresponds exactly to the time necessary for the field to move from the receptor station g_i, with coordinate $\vec{r}_{g_i}$, to the scattering point in subsurface. In this work we have employed the *SEG/EAGE* velocity model (Aminzadeh et al., 1997) to which the image condition for a source point was determined by three methods: Schneider's modified method, which only furnishes the first arrivals; Finite Difference method, which gives the maximum field image condition, and the method proposed herein, that is, by *PARAXIAL* ray-tracing which in this version gives also the *MFIC*. This method is based:

1. In the solution of the kinematic ray-tracing system of equations eq-1, which furnishes the ray trajectories $\vec{x}(\sigma)$ and slowness vector $\vec{p} = \frac{1}{c}$, where dt is the time interval, ds the arc length interval, c the velocity, and σ a parameter given by the second system of equations 1.

2. The dynamical system eq-2 is applied to extrapolate the travel time $T(\vec{x}_0)$ from the ray points to the time $T(\vec{x})$ in the grid points, where $\delta\vec{x}$ and $\delta\vec{p}$ are, respectively, the *variations* of the position and slowness vectors, with respect to the central ray, $\underline{\underline{0}}$ null matrix, $\underline{\underline{I}}$ identity matrix and $\frac{1}{2}\underline{\underline{C}}$ the matrix $\frac{1}{2}\left[\frac{\partial(1/c^2)}{\partial x_i \partial x_j}\right]$ of the second derivatives of the velocity field, all 3×3.

$$\frac{d}{d\sigma}\begin{bmatrix}\vec{x}(\sigma)\\ \vec{p}(\sigma)\end{bmatrix} = \begin{bmatrix}\vec{p}(\sigma)\\ \frac{1}{2}\nabla\left[\frac{1}{c^2(\vec{x}(\sigma))}\right]\end{bmatrix}, \frac{d\sigma}{dT} = c^2(\sigma) = c(\sigma)\frac{d\sigma}{ds} \quad (1)$$

$$\frac{d}{d\sigma}\begin{bmatrix}\delta\vec{x}(\sigma)\\ \delta\vec{p}(\sigma)\end{bmatrix} = \begin{bmatrix}\underline{\underline{0}} & \underline{\underline{I}}\\ \frac{1}{2}\underline{\underline{C}}(\sigma) & \underline{\underline{0}}\end{bmatrix}\begin{bmatrix}\delta\vec{x}(\sigma)\\ \delta\vec{p}(\sigma)\end{bmatrix} \quad (2)$$

In the first stage described above, the kinematic ray-tracing gives the travel time in the ray points $T(\vec{x}_0)$ by the adaptive method, which achieves the magnitude rate of 10^{-6} to the relative error. In the second stage the travel time in the rectangular grid points $T(\vec{x})$ (see fig-1-A) is evaluated by employing the Paraxial ray-tracing system of equations 2. This stage decrements the magnitude rate of the relative error by a factor of 10^{-3}, reaching the same level of the modified Schneider's method.

Summary and Conclusions

1. Figure-2-A shows the *SEG/EAGE* model, a rigorous test to the ray-tracing, because even its smoothness version presents $2200m/s$ of variation in the velocity field along about $100m$ of distance, in the borders of the salt body.
2. Figure-2-B shows the field of maximum amplitude obained during the determination of the finite difference image condition, by using a source frequency of $30HZ$, superimposed to the ray's path. We can perceive the perfect coherence between the regions of higher amplitude values with the regions of higher density of rays, although they are numerical methods of completely distinct conceptions.
3. Figure-2-C shows the maximum field image condition computed by the finite difference method with $30HZ$ of source frequency. The discontinuities in the time field are associated to the fact the maximum amplitude's field can eventually arrive to the grid point after the first arrival.
4. Figure-2-D shows the superposition of the *snapshot* of the finite difference propagating field at time $t = 1.325s$, with the isochronal of the maximum amplitude's field also by the finite difference method. We can see the perfect catching of the maximum field.
5. Figure-2-E shows the modified Schneider's method image condition (Faria and Stoffa, 1994) which determines only the first arrivals, is smooth, doesn't present problems in *shadow zone*, and is fast.
6. Figure-2-F shows the superposition of the *snapshot* at time $t = 1.325s$, with the isochronal of Schneider's method. We can observe that the salt body's scattering field, which has amplitudes several orders of magnitude rate superior than the first arrival, will be lost in the imaging process.
7. Figure-2-G shows the travel time field of the *PARAXIAL* method superimposed to the rays. We can observe the the discontinuities between the region of higher amplitudes of the scattering field and the *shadow zone*.
8. Figure-2-H shows the superposition of the *snapshot* at time $t = 1.325s$, with the isochronal of the maximum amplitude's field obtained by the method proposed herein. The strong amplitudes of the field scattered by the salt body will be incorporated in the image condition contributing to the quality improvement of the depth Kirchhoff's imaging. The arrow points out to a *shadow zone*, where we can see the maximum amplitude catching is not satisfactory. But, In this region the amplitude field is very weak and will not contribute significantly to the migrated field. However, the insertion, if desired, of only one ray can solve this problem without impact in the time of processing, as we can see comparing the *shadow zone* of the left side of fig-2-B (which have only one ray), with the left side of fig-2-H, where the the maximum field was perfectly determined.
9. We can verify that, in regions of geological complexity, part of the imaging deficiency of the Kirchhoff's method when compared to the methods which make use of full wave equations, like *RTM*, can be attributed to the first arrival image condition.
10. In regions of low degree of geological complexity with small variations in the velocity field the image conditions, of maximum field and first arrival, will be almost coincident.
11. Table-1 shows that the maximum field by the Paraxial 2D method was three times slower than the 2D-Schneider's and three times faster for the 3D model.
12. The proposed method in spite of being three times faster than Schneider's furnishes another 36 additional informations to the seismic imaging (AVA, acoustical elastic - Inversion, tomography etc).
13. Table-2 shows a comparison among the travel time field for the three methods, specifically: the correlation factor eq-3, the error expectancy, and the standard deviation. In these calculus it were used all samples, including the *shadow zone*, which favor the Schneider's method. The amplitudes in the *shadow zone* are very small giving a small contribution to the imaging. In this zone the error by the proposed method grows distorting the values to the error expectancy and standard deviation.

$$Corr(\tau, \tau_{ref}) = \frac{\langle\vec{\tau}, \vec{\tau}_{ref}\rangle}{\sqrt{\langle\vec{\tau}, \vec{\tau}_{ref}\rangle\ \langle\vec{\tau}_{ref}, \vec{\tau}_{ref}\rangle}}, \quad (3)$$

References

Alford, R. M., Kelly, K. R., and Boore, D. M., 1974, Accuracy of finite-difference modeling of the acoustic wave equation: Geophysics, **6**, 843–852.

Aminzadeh, F., Brac, J., and Kuns, T., 1997, 3-d salt and overthrust models: SEG/EAGE.

Cunha, P. E. M., 1997, Estratégias eficientes para migração reversa no tempo pré empilhamento 3-D em profundidade pelo método das diferenas finitas: Master's thesis, Universidade Federal da Bahia, Salvador.

Cunha, P. E. M., 1999a, High precision/fast adaptive step size ray-tracing by curvature criteria: Presented at the 6th Ann. Internat. Mtg., Brazilian Geophysical Society, Soc. Expl. Geophys.

——— 1999b, Numerical phase-group velocity anisotropy in finite difference modeling and migration: 6th Ann. Internat. Mtg., Brazilian Geophysical Society, Soc. Expl. Geophys.

Cunha, P. E. M., Migração pré-empilhamento multifocal: Principios, Fundamentos e resultados parciais:, Technical Report TEGG-009/02, PETROBRAS/CENPES/PDEP/TEGG, Rio de Janeiro, CEP 21949-900, jul 2002.

Faria, E. L., and Stoffa, L. P., 1994, Travel time computation in transversely isotropic media: Geophysics, **59**, 272–281.

Mufti, I. R., Pita, J. A., and Huntley, R. W., 1996, Finite-difference depth migration of exploration-scale 3-d seismic data: Geophysics, **61**, 776–794.

Popov, M. M., and Pšenčik, I., 1978a, Computation of ray amplitudes in inhomogeneous media with curved interfaces: Studia geophizika et geodetica, **22**, 248–258.

——— 1978b, Ray amplitudes in inhomogeneous media with curved interfaces.: Geofizikalni Sbornic, **24**, 111–129.

Popov, M. M., 1977, On a method of computation of geometrical spreading in an inhomogeneous medium with interfaces.: Doklady Akdemii Nauk (in Russian), **237**, no. 5.

Popov, M. M., 2002, Ray theory and Gaussian Beam method for geophysicists: CPGG/UFBA, Salvador.

Soares, Filho and Bulcão, André and De Bragança, R. S. N., 2002, Modelagens Sísmicas e Migração RTM em Clusters de Computadores Pessoais: Presented at the XIII Simpósio de geofísica da PETROBRAS, Universidade Corporativa da PETROBRAS.

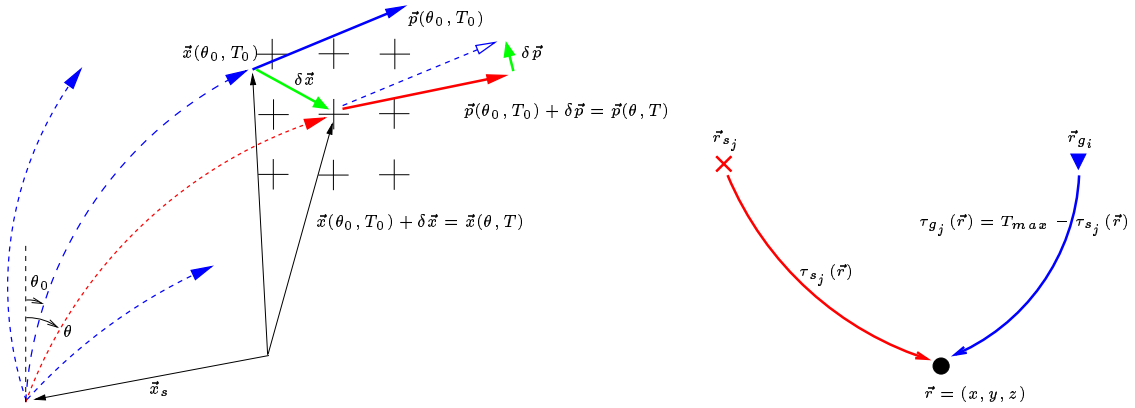

A: Paraxial Ray. B: Punctual source image condition.

Figure 1:

Model	Finite Difference	t: Schneider	t: PARAXIAL	$\frac{T_p}{T_s}$
2D SEG/EAGE	$25s$	$0.410s$	$1.230s$	3.0
3D Model	$14min$	$21.160s$	$6.730s$	.32

Table 1: Processing time by the three methods: Finite Difference, Schneider and the proposed.

$Corr(\tau, \tau_{ref})$	$\tau_s(x,y,z)$ Schneider	$\tau_p(x,y,z)$ PARAXIAL
τ_d: Finite Diff.	$C_{ds} = .999969661$ $E[\lvert\tau_d - \tau_s\rvert] = .00205$ $\sigma_{ds} = .00224$	$C_{dp} = 1.00001717$ $E[\lvert\tau_d - \tau_p\rvert] = .00370$ $\sigma_{dp} = .00584$
τ_s: Schneider	-	$C_{sp} = .999966741$ $E[\lvert\tau_s - \tau_p\rvert] = .00298$ $\sigma_{sp} = .00586$

Table 2: Correlation: Finite Difference, Schneider e *PARAXIAL*.

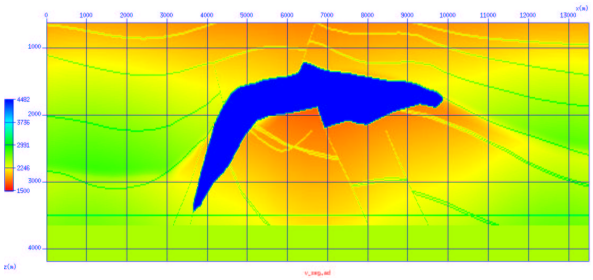

A: *SEG/EAGE* model

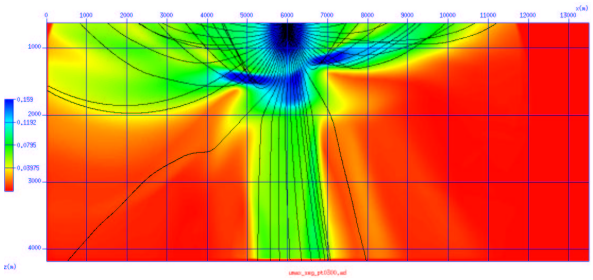

B: Finite difference $A(x,z)$ plus rays

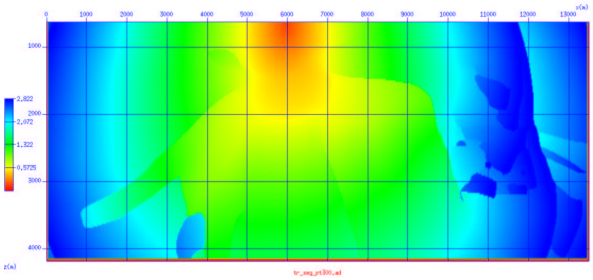

C: $\tau(x,z)$ by Finite difference

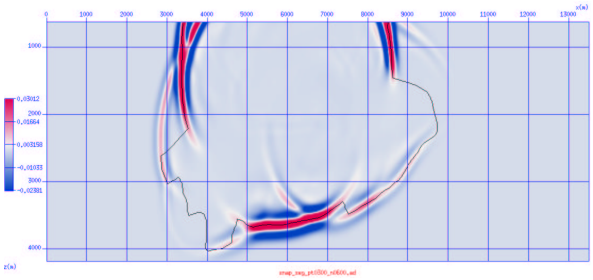

D: isochronal, $t = 1.325$ s

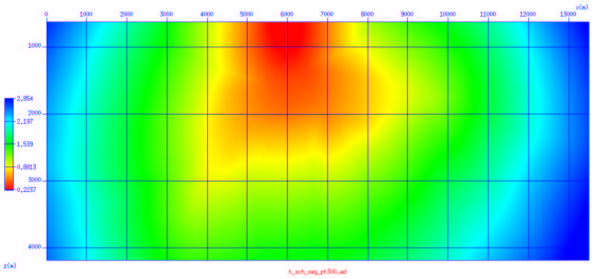

E: $\tau(x,z)$ by Eikonal Schneider's solver

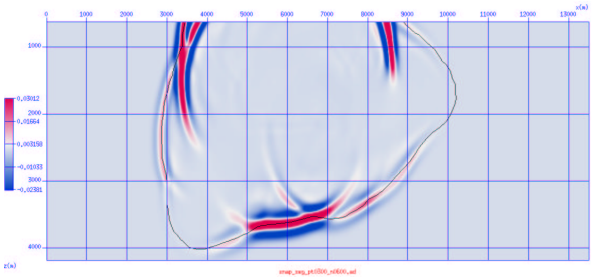

F: isochronal, $t = 1.325$ s

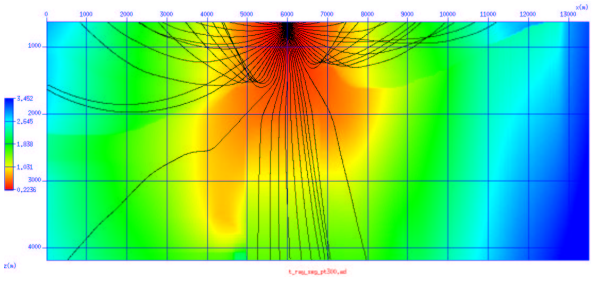

G: $\tau(x,z)$ by Paraxial Ray-tracing

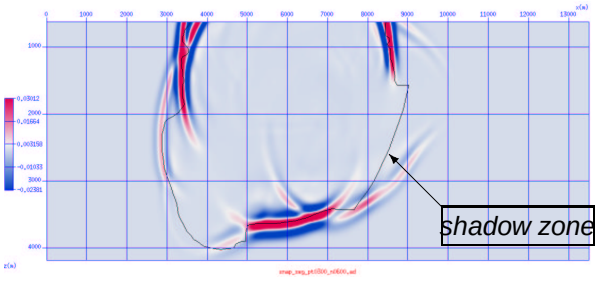

H: isochronal, $t = 1.325$ s

Figure 2: *SEG/EAGE* model: image condition PT0300